Astron. Astrophys. 360, 1031–1042 (2000)

ASTRONOMY AND ASTROPHYSICS

The response of an accretion disc to an inclined dipole with application to AA Tauri

C. Terquem[1,2,3] **and J.C.B. Papaloizou**[4]

[1] Institut d'Atrophysique de Paris, 98 bis Boulevard Arago, 75014 Paris, France (terquem@iap.fr)
[2] Université Denis Diderot-Paris VII, 2 Place Jussieu, 75251 Paris Cedex 5, France
[3] Laboratoire d'Astrophysique, Observatoire de Grenoble, B.P. 53, 38041 Grenoble Cedex 9, France
[4] Astronomy Unit, School of Mathematical Sciences, Queen Mary and Westfield College, Mile End Road, London E1 4NS, UK (J.C.B.Papaloizou@maths.qmw.ac.uk)

Received 14 March 2000 / Accepted 6 June 2000

Abstract. We compute the warping of a disc induced by an inclined dipole. We consider a magnetised star surrounded by a thin Keplerian diamagnetic disc with an inner edge that corotates with the star. We suppose the stellar field is a dipole with an axis that is slightly misaligned with the stellar rotation axis. The rotation axes of the disc material orbiting at large distances from the star and that of the star are supposed to coincide. The misalignment of the magnetic and rotation axes results in the magnetic pressure not being the same on the upper and lower surfaces of the disc. The resultant net vertical force produces a warp which appears stationary in a frame corotating with the star. We find that, if viscosity is large enough ($\alpha \sim 0.01$–0.1) to damp bending waves as they propagate away, a smoothly varying warp of the inner region of the disc is produced. The amplitude of the warp can easily be on the order of ten percent of the disc inner radius for reasonably small misalignment angles (less than 30 degrees). Viscous damping also introduces a phase shift between the warp and the forcing torque, which results in the locations of maximum elevation above the disc forming a trailing spiral pattern. We apply these results to recent observations of AA Tau, and show that the variability of its light curve, which occurs with a period comparable to the expected stellar rotation period, could be due to obscuration produced by a warp configuration of the type we obtain.

Key words: accretion, accretion disks – Magnetohydrodynamics (MHD) – stars: individual: AA Tau – stars: magnetic fields – stars: pre-main sequence

1. Introduction

Objects accreting material through an accretion disc very commonly contain a significant magnetic field. This is the case for accreting white dwarfs in cataclysmic variables, some X–ray binary pulsars and at least some classical T Tauri stars (CCTS).

It was first suggested by Bertout et al. (1988), as a result of the detection of bright stellar spots, that CTTS may accrete along stellar magnetic field lines. This picture has been further supported by a wide array of observational evidence (see Najita et al. 2000 and references therein), including spectroscopic indications of infalling material onto the stellar surface (Edwards et al. 1994; Hartmann et al. 1994) and the low spin rate of CCTS (Bouvier et al. 1993; Edwards et al. 1993).

Since T Tauri stars have a large convective envelope, it is likely that at least part of their magnetic field is generated through a dynamo process. However, there may also be a fossil component originating from the molecular cloud out of which the star formed (Tayler 1987). Recent Zeeman measurements indicate relatively strong field strength at the surface of T Tauri stars, on the order of one kilogauss (Guenther et al. 1999; Johns-Krull et al. 1999). It is not known what the structure of the field is. At some distance from the star the dipolar component probably dominates, but whether this is the case in the magnetosphere is not clear. However, observations cannot rule out such a coherent field structure (Montmerle et al. 1994), and numerical simulations of nonlinear stellar dynamos indicate that a steady dipole mode is the most easily excited one (Brandenburg et al. 1989).

Interaction between the stellar magnetic field and the accretion disc has very important consequences for the disc structure, the accretion process (see Ghosh & Lamb 1991 and references therein) and the evolution of the stellar rotation (Königl 1991). In particular, the disc is truncated by the magnetic torque, so that it does not extend down to the stellar surface (Gosh & Lamb 1979). The location of the disc inner radius is determined by the condition that magnetic and viscous torques balance. For CTTS, the radius of the inner cavity is believed to be a few stellar radii (see, e.g., Wang 1995).

So far, there are only a few numerical simulations of disc–stellar magnetic field interactions (Hayashi et al. 1996; Miller & Stone 1997; Goodson et al. 1997; Kudoh et al. 1999). They all show the disc–magnetosphere interaction to be complex and sensitive to initial and boundary conditions. At this stage, it is not clear what final form a full theoretical model is likely to take. However, analytical or semi–analytical simplified models can still be valuable in pointing out some important processes

Send offprint requests to: C. Terquem

that may arise in these systems, and the goal of this paper is to describe one of these processes.

We note that the magnetic axis and the rotation axis of the disc at large distances from the star may not be aligned, although often, for simplicity, they are assumed to coincide. We assume here that the stellar rotation axis and the disc rotation axis at large distances coincide. Misalignment would then occur if, for instance, the star were to generate a dipole field with magnetic axis misaligned with its spin axis (like in the case of the Earth). It is possible that the interaction with the disc would lead to some evolution of the misalignment angle, but the details are likely to depend on the processes which generate the field. In any case, when such a misalignment is present, the magnetic pressure is not the same on the upper and lower surfaces of the disc. This mismatch generates a net vertical force which excites bending waves and warps inner parts of the disc (Aly 1980).

Bending instabilities in a disc subject to a stellar magnetic dipole have been investigated by Agapitou et al. (1997, hereafter APT). APT calculated the global bending modes of a disc permeated by both an internally produced poloidal magnetic field and an external dipole field with axis aligned with the disc rotation axis (in this case no warp is induced by the dipole configuration, but free bending modes can be excited by a perturbation which takes the disc out of its equilibrium plane). They found that instability could occur if the magnetic and centrifugal forces were comparable in some region of the disc. They pointed out that such instabilities may result in the periodic variability observed in the light curve of many CTTS.

Lai (1999) studied the warping of a disc induced by an inclined dipole. He calculated the magnetic torque exerted by an inclined dipole on a disc, and studied the stability against vertical displacements of a disc subject to such a torque. In the terms of the APT analysis, he studied the stability of low frequency (as measured in an inertial frame) bending modes corresponding to the modified tilt mode as discussed in APT. We note that, when considering the structure of the disc subject to the inclined dipole, he did not take into account the effects of the distortion of the disc itself on its response, which can have important consequences on the dynamics through wave propagation. But he added the effects of a toroidal field, assumed to be generated by winding up a penetrating vertical field, on the magnetic pressure determining the vertical force on the disc. This contribution is phase shifted with respect to the other contributions and may thus (if not counteracted) cause the modified tilt mode to become unstable, resulting in spontaneous warping. To decide whether this mode can be destabilised requires detailed consideration of the effects of wave propagation and viscosity. We comment that under some conditions warps diffuse away on a timescale much shorter than the viscous timescale (Papaloizou & Pringle 1983) or propagate away with a velocity on the order of the sound speed (Papaloizou & Lin 1995) resulting in stabilisation.

In this paper, we calculate the structure of a thin Keplerian disc subject to an inclined dipole, taking into account the effects of the distortion of the disc itself on its response, i.e. the full dynamics of the system. For simplicity, we suppose that the disc is diamagnetic, so that it is not permeated by the external stellar field. In principle, the calculations presented here could be extended to more general cases. However, if the disc were not diamagnetic, wrapping of field lines would probably become important, leading to the possible disruption of the magnetosphere (see, e.g., Mikic & Linker 1994). Also we do not address here the physical processes of accretion or plasma entry into the stellar magnetosphere. We note that because the warp induced in the inner disc appears steady in a frame rotating with the star, any resulting variability would have the same period as that of the star.

We comment that the generation of spontaneous warping does not apply to the calculations we present here, since we study a response which is forced by the inclined dipole and has a pattern speed equal to the rotation rate of the star. Thus, in contrast to the considerations of Lai (1999), it is not a modified tilt mode.

This work has been motivated by a recent study of Bouvier et al. (1999) who report that the light curve of the CTTS AA Tau displays photometric, spectroscopic and polarimetric variations on timescales from a few hours to several weeks. The most striking feature of this light curve is a photometric variability with a period comparable to the expected rotation period of the star. This has been interpreted by Bouvier et al. (1999) as being due to the occultation of the star by a warp of the inner disc (the system is observed almost edge–on). The authors speculated that the warp could be produced by an inclined dipole. We note that Bouvier et al. (1999) did not consider AA Tau as being a special case as far as its properties are concerned. They pointed out that only its light curve is unusual, and they interpreted it as being due to the fact that the system is seen almost edge–on. In other words, warping of the inner parts of CTTS discs would not be uncommon, but it could be seen only for particular viewing angles.

The plan of the paper is as follows: We begin by considering an equilibrium configuration where the axis of the dipole and the rotation axis of the disc are aligned. This is described in Sect. 2. We then perturb this equilibrium by slightly inclining the dipole. In Sect. 3 we calculate the resulting perturbed magnetic field and derive the integro–differential equation which has to be solved for the disc vertical displacement. This equation is solved in the WKB approximation, which is valid when the wavelength of the bending waves excited in response to the perturbation is small compared to the disc radius. To allow these waves to damp as they propagate away (and therefore to damp very small wavelength oscillations, which would be unphysical), we include the effects of viscous damping in the integro–differential equation. In Sect. 4 we solve this equation numerically and present the results for two different magnetic field equilibria (derived by Aly 1980 and Low 1986). In both cases we find that, if the viscosity is large enough to damp the waves as they propagate away, a smooth warp configuration of the disc inner parts can exist. The elevation above the disc equilibrium plane (i.e. the stellar equatorial plane) can easily be on the order of ten percent of the disc inner radius for reasonably small misalignment angles (less than 30 degrees). If the viscosity is too small to damp the waves efficiently, the disc inner parts may be disrupted, and it

is likely that the evolution is then highly time–dependent. In Sect. 5 we apply these results to the case of AA Tau, and show that the variability of its light curve, which occurs with a period expected to be the stellar rotation period, can plausibly be explained by a warp configuration of the type we obtain.

2. Disc and aligned dipole

We begin by considering a thin disc configuration such that the gas orbits a central rotating star with a dipole field and where the magnetic axis and rotation axes are all aligned. In this situation, the configuration is axisymmetric. For convenience, we work in a frame corotating with the central star with angular velocity ω. The disc is truncated in its inner parts by the magnetic torque and we will suppose that the inner edge corotates with the star.

2.1. Magnetic field

The dipole field $\mathbf{B}_{ext}$ due to the central star induces azimuthal currents in the conducting disc which in turn generate an additional poloidal magnetic field $\mathbf{B}_d$.

Here, as in APT, we shall assume that the field external to the disc and central star can be approximated as curl free, i.e. assumed to be a vacuum field (the currents external to the disc and star are at infinity).

The total axisymmetric poloidal magnetic field, $\mathbf{B}_{ext}+\mathbf{B}_d$, is denoted $\mathbf{B} = (B_r, 0, B_z)$, where we use cylindrical polar coordinates (r, φ, z). The associated Cartesian coordinates are (x, y, z). The flux function ψ is such that:

$$B_r = \frac{-1}{r}\frac{\partial \psi}{\partial z} \text{ and } B_z = \frac{1}{r}\frac{\partial \psi}{\partial r}. \quad (1)$$

For the stellar dipole field:

$$\psi_{ext} = -\frac{\mu_d r^2}{(r^2+z^2)^{3/2}}, \quad (2)$$

where the magnitude of the stellar magnetic dipole moment is $\mu_d = B_* R_*^3$, with B_* and R_* being the stellar magnetic field and radius, respectively.

For the general axisymmetric poloidal field, the associated current density is $\mathbf{j} = (0, j_\varphi, 0)$. For an infinitesimally thin disc, as we consider here, we define the vertically integrated azimuthal component of the current density, J, such that:

$$J = \int_{-\infty}^{\infty} j_\varphi \mathrm{d}z.$$

By integrating the azimuthal component of Ampère's law through the disc, we obtain:

$$B_r^+ = \mu_0 J/2, \quad (3)$$

where B_r^+ denotes the radial component of the magnetic field just outside the upper surface of the disc. Throughout this paper we use MKSA units, and μ_0 denotes the permeability of the vacuum. B_r is antisymmetric with respect to reflection in the disc mid–plane so that its value just outside the lower surface of the disc is $B_r^- = -B_r^+$.

2.2. Force balance

Neglecting pressure forces as in APT, the vertical integration of the radial component of the momentum equation yields the condition for radial equilibrium as:

$$\Sigma \frac{\partial \Phi}{\partial r} = \Sigma r \Omega^2 + J B_z, \quad (4)$$

where Σ is the surface density, Ω is the disc angular velocity measured in an inertial frame, and Φ is the gravitational potential here taken to be due to a central point mass, M_*, such that:

$$\Phi = -\frac{GM_*}{\sqrt{r^2+z^2}}.$$

If $B_z \neq 0$, in some regions of the disc a variety of configurations are possible (see APT). These include cases where inner field lines cross the disc and join to the central star and thus may be assumed to corotate with it. Outer field lines may be open in the case of an infinite disc or a finite disc with appropriate boundary conditions.

In this paper, for simplicity, we shall perform calculations for the special case where the field is excluded from the disc. This situation arises when the disc is perfectly conducting. Then only surface currents flow in the disc and they screen the stellar dipole field from the disc interior, i.e. they produce an additional field $\mathbf{B}_d$ which cancels $\mathbf{B}_{ext}$ in the disc interior. We note that, since the vertical component of the field is continuous at the disc surface, B_z just outside the disc is zero in this case. The same does not apply for B_r, and in general B_r^+ and B_r^- are non zero.

We remark that, since there is no Lorentz force acting in the disc when $B_z = 0$, the angular velocity given by Eq. (4) is Keplerian.

3. Disc and slightly misaligned dipole

We suppose that the system is perturbed from the axisymmetric equilibrium state described above by introducing a slight misalignment between the magnetic axis of the central dipole and the rotation axis of the disc and star (the z axis). This produces a non axisymmetric response in the disc that can be described using linear perturbation theory.

The main features of this response is that it takes the form of a warping of the disc, as indicated by Aly (1980), together with the additional feature of the excitation of bending waves. The response is naturally largest in the inner parts of the disc where the magnetic field is strongest. As we indicate by considering specific examples in Sect. 4, it can take the form of a steeply changing inclination of the inner disc orbits which can make it appear to have an inner wall.

To calculate the geometry of the disc (that is its elevation above its equilibrium plane), we extend the analysis of APT. To compute the free bending modes of the disc, APT solved an eigenvalue problem where the eigenvalues were the mode frequencies and the eigenfunctions their amplitudes. Here we are interested in a response with frequency equal to that of the forcing term. Since the dipole is anchored in the star, this is

the angular velocity of the star. The amplitude of the mode (its spatial dependence) can be found from the mode equation of APT with a specified frequency and the addition of the forcing term. However, a different equilibrium field is adopted, since here, in contrast to APT, there is no internally produced field in the disc.

3.1. Perturbed magnetic field

To calculate the response we suppose the central dipole moment is rotated in the (x, z) plane through a small angle δ being the inclination to the z axis. The dipole moment is then given by:

$$\boldsymbol{\mu}_d = (\mu_d\delta, 0, \mu_d). \tag{5}$$

This contributes to a potential:

$$\Phi'_{\mathrm{M},ext} = \frac{\boldsymbol{\mu}_d \cdot \mathbf{r}}{|\mathbf{r}|^3}, \tag{6}$$

where $\mathbf{r}$ denotes the position vector, which produces a radial external magnetic field perturbation $B'_{r,ext} = \partial\Phi'_{\mathrm{M},ext}/\partial r$. Just outside the disc surfaces, this is given by the real part of:

$$B'^{+}_{r,ext} = B'^{-}_{r,ext} = -\frac{2\mu_d\delta\exp(i\varphi)}{r^3}. \tag{7}$$

Thus the problem reduces to the calculation of the disc response to a field perturbation with azimuthal mode number $m = 1$. This, when acting with the unperturbed azimuthal current, produces a vertical Lorentz force which tends to warp the disc. In other terms, when the dipole is misaligned, the magnetic pressure force is not the same on the upper and lower surfaces of the disc. This mismatch generates a net vertical pressure force which tends to warp the disc.

We thus introduce the Lagrangian displacement $\boldsymbol{\xi}$ which, in a razor–thin disc approximation, has the form:

$$\boldsymbol{\xi} = (0, 0, \xi_z).$$

The only non-negligible component is the vertical one (APT), and ξ_z represents the elevation above the disc equilibrium plane. In keeping with the form of the external magnetic field perturbation, we make all the perturbed quantities complex by taking their φ-dependence to be through a factor $\exp(i\varphi)$, which henceforth will be dropped. The physical perturbations will be recovered by taking the real part of these complex quantities. The Eulerian perturbations of the various quantities are denoted by a prime.

The perturbation of the magnetic field interior to the disc, $\mathbf{B}'$, is related to $\boldsymbol{\xi}$ by the flux freezing condition:

$$\mathbf{B}' = (B'_r, B'_\varphi, B'_z) = \boldsymbol{\nabla}\times(\boldsymbol{\xi}\times\mathbf{B}). \tag{8}$$

The non-zero components of $\mathbf{B}'$ take the form:

$$B'_r = -\xi_z\frac{\partial B_r}{\partial z}, \text{ and } B'_z = \frac{1}{r}\frac{\partial(rB_r\xi_z)}{\partial r}. \tag{9}$$

Since B_r is antisymmetric with respect to reflection in the disc mid–plane and ξ_z is independent of z in the thin disc approximation, B'_z is antisymmetric and B'_r is symmetric.

As in APT, the vertical component of the perturbed field must be matched to the vertical component of a perturbed vacuum field exterior to the disc. Here this is taken to be a potential field. Therefore we have:

$$\frac{\partial\Phi'_{\mathrm{M}}}{\partial z} = B'^{+}_z, \tag{10}$$

where B'^{+}_z is the value of the vertical field perturbation just outside the disc surface and Φ'_{M} is the magnetic potential associated with the external field perturbation. To find Φ'_{M}, we first subtract out the contribution of the external field perturbation arising from the tilted dipole. At the disc surface, this is (Eq. [6]):

$$\Phi'_{\mathrm{M},ext} = \frac{\mu_d\delta}{r^2}, \tag{11}$$

where as above the factor $\exp(i\varphi)$ has been dropped. With this contribution removed, the residual potential has no singularity outside the disc. It can be calculated from Eq. (10) in an analogous manner to finding the gravitational potential due to a disc surface density distribution, with $2\pi G\Sigma$ (where G is the gravitational constant) being replaced by B'^{+}_z (see Tagger et al. 1990; Spruit et al. 1995; APT). Following this procedure, Φ'_{M} may be written as the sum of a Poisson integral and $\Phi'_{\mathrm{M},ext}$:

$$\Phi'_{\mathrm{M}} = \Phi'_{\mathrm{M},d} + \Phi'_{\mathrm{M},ext}, \tag{12}$$

where

$$\Phi'_{\mathrm{M},d} = -\frac{1}{2\pi}\int_{R_i}^{R_o}\int_0^{2\pi}\frac{B'^{+}_z(r')\cos\varphi'\ r'\mathrm{d}r'\mathrm{d}\varphi'}{\sqrt{r'^2 + r^2 - 2rr'\cos(\varphi') + z^2}}, \tag{13}$$

where R_i and R_o are the inner and outer radii of the disc, respectively. In the above integral, the φ-dependence of the perturbed field has been taken into account. Here again, the factor $\exp(i\varphi)$, to which $\Phi'_{\mathrm{M},d}$ is proportional, has been dropped.

Since the disc is perfectly conducting, the vertical component of the field given by Eq. (9) is continuous at the disc surface. Therefore:

$$B'^{+}_z = \frac{1}{r}\frac{\partial(rB^{+}_r\xi_z)}{\partial r}. \tag{14}$$

This expression for B'^{+}_z can be used in the above integral.

The radial component of the magnetic field just outside the surfaces of the disc is given by:

$$B'^{+}_r = B'^{-}_r = \left(\frac{\partial\Phi'_{\mathrm{M}}}{\partial r}\right)_{z=0} = \left(\frac{\partial\Phi'_{\mathrm{M},d}}{\partial r}\right)_{z=0} - \frac{2\mu_d\delta}{r^3}, \tag{15}$$

where Eqs. (11) and (12) have been used to write the last expression (we have approximated the derivatives at the disc surfaces by their value at $z = 0$ because the disc is infinitesimally thin).

3.2. The disc vertical displacement

The vertical component of the perturbed Lorentz force integrated vertically through the disc is (see APT):

$$\int_{-\infty}^{\infty} F'_z\mathrm{d}z = -\frac{2B^{+}_r B'^{+}_r}{\mu_0}. \tag{16}$$

The term proportional to $\partial B_z/\partial r$, which was present in APT, is zero here since $B_z = 0$ in the disc interior and at its surfaces (see Sect. 2.2).

We note that this force is simply the perturbed magnetic pressure force P'_m vertically integrated through the disc. The pressure force vertically integrated through the disc is indeed:

$$P_m = -\frac{(B_r^+)^2}{2\mu_0} + \frac{(B_r^-)^2}{2\mu_0}, \tag{17}$$

($B_z = 0$ at the disc surfaces), so that:

$$P'_m = -\frac{B_r^+ B_r'^+}{\mu_0} + \frac{B_r^- B_r'^-}{\mu_0} = -\frac{2B_r^+ B_r'^+}{\mu_0}, \tag{18}$$

where we have used the symmetries of the field. We note that P'_m is non zero because the perturbation induced by the misaligned dipole has an opposite effect on the upper and lower surfaces of the disc: it increases the magnitude of the radial component of the magnetic field on one of the surfaces from $|B_r^+|$ to $|B_r^+| + |B_r'^+|$ while decreasing it on the other surface from $|B_r^+|$ to $|B_r^+| - |B_r'^+|$.

The vertically integrated z-component of the perturbed equation of motion is:

$$\Sigma \frac{\mathrm{D}^2\xi_z}{\mathrm{D}t^2} = -\Sigma \left(\frac{\partial^2 \Phi}{\partial z^2}\right)_{z=0} \xi_z + \int_{-\infty}^{\infty} F'_z \mathrm{d}z \tag{19}$$

where $\mathrm{D}/\mathrm{D}t$ denotes the convective derivative.

In the problem considered here, the solution is steady in a frame rotating with the central star angular velocity ω. Then:

$$\Sigma \frac{\mathrm{D}^2\xi_z}{\mathrm{D}t^2} = -\Sigma(\omega - \Omega)^2 \xi_z. \tag{20}$$

Also, for a point mass potential:

$$\left(\frac{\partial^2 \Phi}{\partial z^2}\right)_{z=0} = \frac{GM}{r^3} = \Omega_{\mathrm{K}}^2, \tag{21}$$

where Ω_{K} is the Keplerian angular velocity. Using Eqs. (15), (16), (20) and (21), Eq. (19) becomes:

$$\left[-(\omega - \Omega)^2 + \Omega_{\mathrm{K}}^2\right] \xi_z = -\frac{2B_r^+}{\mu_0 \Sigma} \left[\left(\frac{\partial \Phi'_{\mathrm{M},d}}{\partial r}\right)_{z=0} - \frac{2\mu_d \delta}{r^3}\right]. \tag{22}$$

The potential $\Phi'_{\mathrm{M},d}$ can be expressed in term of ξ_z and its derivative with respect to r using Eqs. (13) and (14). Therefore Eq. (22) gives a linear equation for determining the vertical displacement ξ_z induced by the tilted external dipole. The term proportional to μ_d in this equation acts like a forcing term for the vertical displacement and it causes the disc to become warped and may also excite bending waves.

As noted above, since there is no Lorentz force acting in the disc interior, Ω in Eq. (22) is the Keplerian angular velocity.

We remark that Eq. (22) is the same as Eq. (14) of APT with $B_z = 0$, but with an additional nonhomogeneous term proportional to μ_d. As noted above, this is expected as here we calculate the response which is forced by the nonaligned dipole. We remark that this nonhomogeneous term is simply the pressure force due to the misaligned component of the dipole vertically integrated through the disc:

$$P'_{m,ext} = -\frac{2B_r^+ B_{r,ext}'^+}{\mu_0} = \frac{2B_r^+}{\mu_0} \frac{2\mu_d \delta}{r^3}, \tag{23}$$

where we have used Eq. (7) (see also Eq. [24] of Aly 1980).

3.3. WKB waves

When μ_d is set to zero in Eq. (22), this equation has solutions corresponding to free bending waves. In the local limit, these can be found by assuming that $\xi_z \propto \exp(ikr)$, where k is the radial wavenumber, assumed to be very large compared to $1/r$. The integral in Eq. (13) can be evaluated in the WKB approximation to give, after using (14) (see APT and references therein):

$$\Phi'_{\mathrm{M}} = \frac{-B'_z}{|k|} = \frac{-ikB_r^+ \xi_z}{|k|}. \tag{24}$$

The local dispersion relation derived from Eq. (22) is then:

$$(\omega - \Omega_{\mathrm{K}})^2 = \Omega_{\mathrm{K}}^2 + \frac{2(B_r^+)^2}{\mu_0 \Sigma}|k|, \tag{25}$$

where we have used the fact that the angular velocity is Keplerian. We see from Eq. (25) that bending waves with $m = 1$ propagate (with $|k| > 0$) exterior to the Lindblad resonances where $(\omega - \Omega_{\mathrm{K}}) = \pm\Omega_{\mathrm{K}}$. In this paper, we are concerned with the situation where the disc is terminated at an inner boundary ($r = R_i$) where the local Keplerian rotation rate is close to corotation with the central star, i.e. $\Omega_{\mathrm{K}}(R_i) = \omega$. In such a case, only the outer Lindblad resonance (OLR), where $\Omega_{\mathrm{K}} = \omega/2$, will exist within the disc, and it occurs at a radius $r = 1.59R_i$.

Significantly beyond the OLR, the wavenumber associated with the waves is given by:

$$|k|r \sim \frac{\mu_0 \omega^2 r \Sigma}{2(B_r^+)^2} \propto \frac{r^3}{\beta}, \tag{26}$$

where we define β such that it would be the ratio of magnetic to centrifugal forces if we had a vertical field $B_z \sim B_r^+$ (see Sect. 4). Although $B_z = 0$ here, we use β as a measure of the strength of B_r^+. This is expected to be at most of order unity at the inner edge of the disc and then to decrease rapidly outwards, as the magnetic field decreases (see Sect. 4).

If β decreases as r increases, the forcing term proportional to μ_d in Eq. (22) will excite bending waves in the disc that propagate outwards with increasing wavenumber until they are damped, much as in the case of Saturn's rings (see Goldreich & Tremaine 1978; Shu 1984). In some cases, the wavelength may be so short at the OLR that dissipative processes prevent waves from being properly launched (see below).

3.4. Viscous dissipation

In order to allow the waves to damp as they propagate away from the OLR, we add an additional viscous force per unit mass to

the right hand side of Eq. (19) of the form $\nu\partial^2 v'_z/\partial r^2$, where v'_z is the Eulerian perturbed vertical velocity and ν is a kinematic viscosity. Neglecting the variation of Ω_K, which is reasonable for short wavelength disturbances, this can also be written as $i\nu(\Omega_{\rm K}-\omega)\partial^2\xi_z/\partial r^2$. For ν we use a standard 'α' prescription such that $\nu=\alpha H^2\Omega_{\rm K}$, where H is the disc semi–thickness and α is a constant (Shakura & Sunyaev 1973).

With the incorporation of the above viscous force, Eq. (22), which gives the forced response of the disc, becomes:

$$\left[-(\omega-\Omega)^2+\Omega_{\rm K}^2\right]\xi_z - i\nu(\Omega_{\rm K}-\omega)\frac{\partial^2\xi_z}{\partial r^2} = -\frac{2B_r^+}{\mu_0\Sigma}\left[\left(\frac{\partial\Phi'_{{\rm M},d}}{\partial r}\right)_{z=0}-\frac{2\mu_d\delta}{r^3}\right]. \quad (27)$$

We now comment briefly on the possible origin of this α viscosity. So far, the only process which has been shown to initiate and sustain turbulence in Keplerian discs is the magnetohydrodynamic Balbus–Hawley instability, and it does lend itself to an α formalism (Balbus & Hawley 1998 and references therein). For the disc we consider here, which is not permeated by the external magnetic field, it is difficult to justify the existence of an α viscosity. However, in reality, the disc is probably permeated to at least a small extent by the external field (Ghosh & Lamb 1979). If the ratio of magnetic to thermal pressure is smaller than unity, the disc is then subject to the BH instability, the internal disc field is amplified and bending waves are damped. The values of α produced by the BH instability range roughly from 10^{-3} to 0.1 (Hawley et al. 1995; Brandenburg et al. 1995), the largest values corresponding to the case where the magnetic field varies on a scale large compared to the disc semithickness (Hawley 2000).

4. Numerical response calculations

4.1. Unperturbed magnetic field

For the model calculations presented here, we adopt a radial magnetic field corresponding to the situation when the central dipole flux is completely excluded from the disc. We consider both the solutions computed by Aly (1980) and Low (1986). Aly's solution corresponds to the case when all the dipole flux goes through the magnetospheric cavity in the middle of the disc, and is singular at the disc inner edge. Low gives a solution that is non singular with some flux escaping to infinity.

In these cases we have, for r larger than some radius r_B:

$$B_r^+ = \mp B_0\left(\frac{R_o}{r}\right)^3\left[\left(\frac{r}{r_B}\right)^2-1\right]^{\pm 1/2}, \quad (28)$$

where we have defined:

$$B_0=\frac{4\mu_d}{\pi R_o^3}. \quad (29)$$

In Eq. (28), the upper sign corresponds to Low's solution, whereas the lower sign corresponds to Aly's solution. Of course, in both cases $B_z=0$ since the disc is diamagnetic. Note that the radial field at the disc surface has opposite sign in the two cases.

We comment that B_r^+ is negative and positive for Low's and Aly's cases, respectively, which is the opposite of the solution obtained by these authors. This is because we have arbitrarily chosen B_z to be positive when the dipole moment μ_d is positive, in contrast to these authors.

In a two dimensional model, r_B is the disc inner radius. However, more realistically it is expected to differ from this by an amount comparable to the vertical thickness of the disc. We adopted the procedure of taking the disc inner radius R_i to be slightly larger than r_B, and to check convergence of the results by decreasing (R_i-r_B). For Aly's solution, convergence requires that the disc surface density increases rapidly enough towards R_i such as to limit the Lorentz force there.

4.2. Results

We have performed global normal mode calculations for disc models with the unperturbed magnetic field described above.

We solve Eq. (27) considered as an integro-differential equation for the response function ξ_z by the method described in APT. We use the dimensionless radius $\varpi=r/R_o$, so that the outer radius is $\varpi_o=1$. In these units, the disc inner radius on the computational grid is taken to be $\varpi_i=R_i/R_o=0.1$, and to corotate with the central star so that $\omega=\Omega_K(R_i)$.

The radial interval $[\varpi_i,1]$ is divided into a grid of n_r equally spaced points at positions $(\varpi_I)_{I=1...n_r}$ with a spacing $\Delta\varpi_I=\varpi_{I+1}-\varpi_I$. Eq. (27) is solved as in APT by discretizing it on the grid so converting it into a matrix inversion problem for $(\xi_z)_{I=1...n_r}$. In the calculations presented below, n_r was varied between 500 and 700, but 300 already gave satisfactory results.

As already noted in Sect. 3.3, we use the magnetic support β, which would be the ratio of the Lorentz force to the centrifugal force in the disc if B_z were non zero and on the order of B_r^+:

$$\beta=\frac{2\left(B_r^+\right)^2 r^2}{\mu_0\Sigma G M_*}, \quad (30)$$

where G is the gravitational constant. Although $B_z=0$ in the disc, β will be used as a measure of the strength of the field B_r^+. We found it convenient to define the dimensionless quantities $\bar\Sigma=\Sigma/\Sigma_i$, where Σ_i is the surface density at the disc inner radius, $\bar B_r^+=B_r^+/B_0$, and $\bar\beta=\beta/\beta_0$ with:

$$\beta_0=\frac{B_0^2R_o^2}{\mu_0\Sigma_i G M_*}. \quad (31)$$

We then have:

$$\bar\beta=\frac{2\varpi^2\left(\bar B_r^+\right)^2}{\bar\Sigma}. \quad (32)$$

For both Low's and Aly's magnetic field, we consider models where the magnetic support is large (reaching values of order unity) close to the disc inner edge and decreases rapidly with radius. For Aly's solution, we take $\beta=1$ at the disc inner edge. For Low's solution, β has to vanish at the same location as B_r^+, i.e. at $\varpi_B=r_B/R_o$, otherwise ξ_z is infinite there. We then

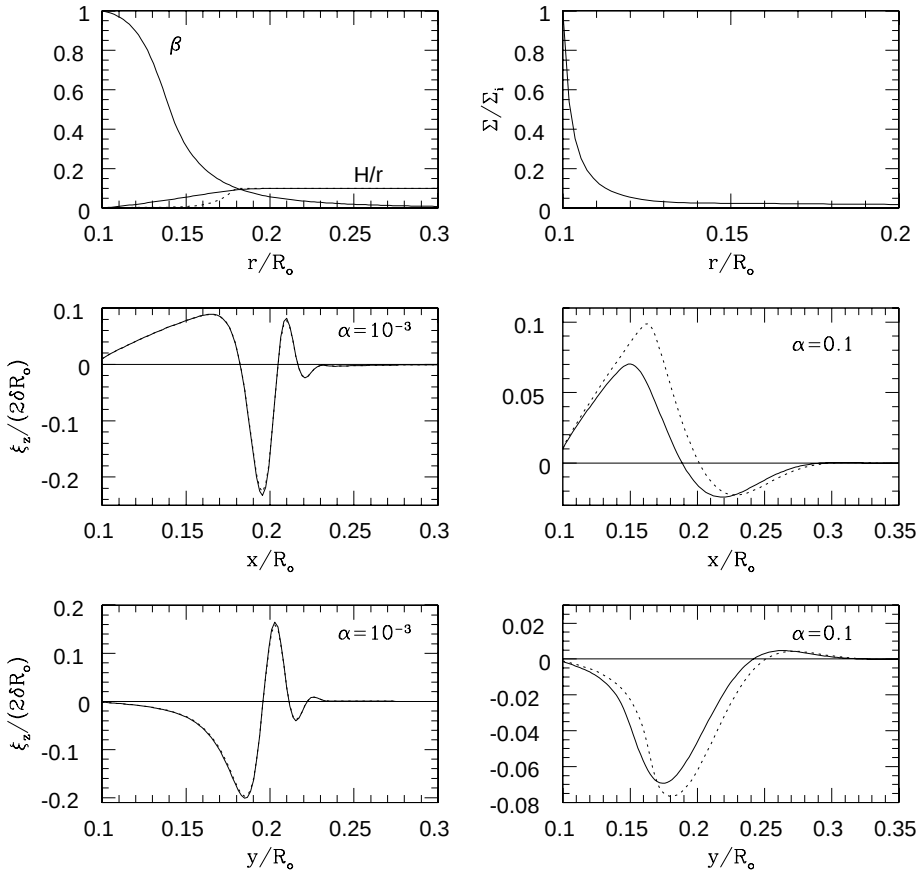

Fig. 1. Results for Aly's magnetic field. *Top left panel:* Magnetic support β and aspect ratio H/r for an almost linear (*solid line*) and exponential (*dotted line*) profile versus $\varpi = r/R_o$. *Top right panel:* Surface density Σ/Σ_i where $\Sigma_i = \Sigma(R_i)$ versus $\varpi = r/R_o$ *Middle panels:* $\mathcal{R}(\xi_z)/(2\delta R_o)$, i.e. $\xi_z/(2\delta R_o)$ for $\varphi = 0$ versus x/R_o. *Bottom panels:* $-\mathcal{I}(\xi_z)/(2\delta R_o)$, i.e. $\xi_z/(2\delta R_o)$ for $\varphi = \pi/2$ versus y/R_o. The different curves are for $\alpha = 10^{-3}$ (*left panels*) and 0.1 (*right panels*) and correspond to the almost linear (*solid lines*) and exponential (*dotted lines*) profile of H/r. Here $\varpi_B = 0.0975$. Only the inner parts of the disc where the displacement is non zero are shown. Several oscillations corresponding to bending waves excited at the OLR are visible for $\alpha = 10^{-3}$. These are damped by viscosity before they propagate very far.

take $\beta = 0$ at ϖ_B and $\beta = 1$ at the location where B_r^+ has its maximum. From the value of β and $\bar{B}_r^+$ at the disc inner radius, we can calculate β_0.

From the profile of $\bar{\beta}$, we calculate $\bar{\Sigma}$ using Eq. (32). We actually take the profile of $\bar{\Sigma}$ which gives the desired $\bar{\beta}$ near the disc inner edge, and we then match it on to a $r^{-3/2}$ profile further away in the disc (since B_r^+ decreases rapidly with radius, we do not need to worry about the profile of Σ for ϖ larger than a value which turns out to be about 0.2).

We note that our results do not depend on the numerical values of Σ_i, B_0, and R_i (or equivalently R_o) taken individually, but only on β_0 and δ. For R_i we could take a few times R_*, and then compute $R_o = 10R_i$. We could then get a value of B_0 by using Eq. (29) with $\mu_d = B_* R_*^3$. Then Σ_i would follow from the expression (31) for β_0. Depending on the value of Σ_i, the amount of mass in the annulus between R_i and R_o could be modified by changing the profile of $\bar{\Sigma}$ for $\varpi > 0.2$.

An external poloidal magnetic field tends to squeeze the disc. Therefore, we choose a form of the aspect ratio H/r which is zero at the disc inner edge and which increases as the magnetic support decreases. The disc is squeezed by the magnetic field if the magnetic pressure dominates over the thermal pressure. If the sound speed is about a tenth of the Keplerian velocity, then the magnetic and thermal pressures become comparable when the magnetic support is about 0.1. Therefore, we choose a profile of H/r which reaches a constant value (that we take to be 0.1) at the location where $\beta = 0.1$.

We note that the vertical displacement of the disc at a location (r, φ) is:

$$\mathcal{R}[\xi_z(r)] \cos\varphi - \mathcal{I}[\xi_z(r)] \sin\varphi. \tag{33}$$

Figs. 1–3 show the magnetic support β, the disc aspect ratio H/r and the surface density Σ/Σ_i versus ϖ. Also displayed are $\mathcal{R}(\xi_z)/(2\delta R_o)$, i.e. $\xi_z/(2\delta R_o)$ for $\varphi = 0$ versus x/R_o, and $-\mathcal{I}(\xi_z)/(2\delta R_o)$, i.e. $\xi_z/(2\delta R_o)$ for $\varphi = \pi/2$ versus y/R_o, for $\alpha = 10^{-3}$ and 0.1. These quantities represent the disc vertical displacement within a factor $2\delta R_o$ in the $(\varphi = 0)$ and $(\varphi = \pi/2)$ half planes, respectively, or, equivalently, in the $(x > 0, z)$ and $(y > 0, z)$ half planes, respectively (see Eq. [33]). The different figures correspond to different models.

Figs. 1 and 2 correspond to Aly's solution and $\varpi_B = 0.0975$. In Fig. 1, $1/\beta \propto \exp[100(\varpi - 0.14)] + 1$. The results do not depend significantly on the details of the H/r profile in the disc inner parts (we considered both the case where H/r increases almost linearly and exponentially with radius). We also checked that ξ_z hardly changes when ϖ_B varies between 0.09 and 0.099, providing we keep the same magnetic support (i.e. we change Σ accordingly). Fig. 2 corresponds to $\beta \propto B_r^+ / \{\exp[40(\varpi - 0.14)] + 1\}$. The results are qualitatively the same as in Fig. 1. We also ran the case $\beta \propto 1/\varpi^3$, which gave similar results, except that the positive values reached by ξ_z in that case were almost as large as the negative values.

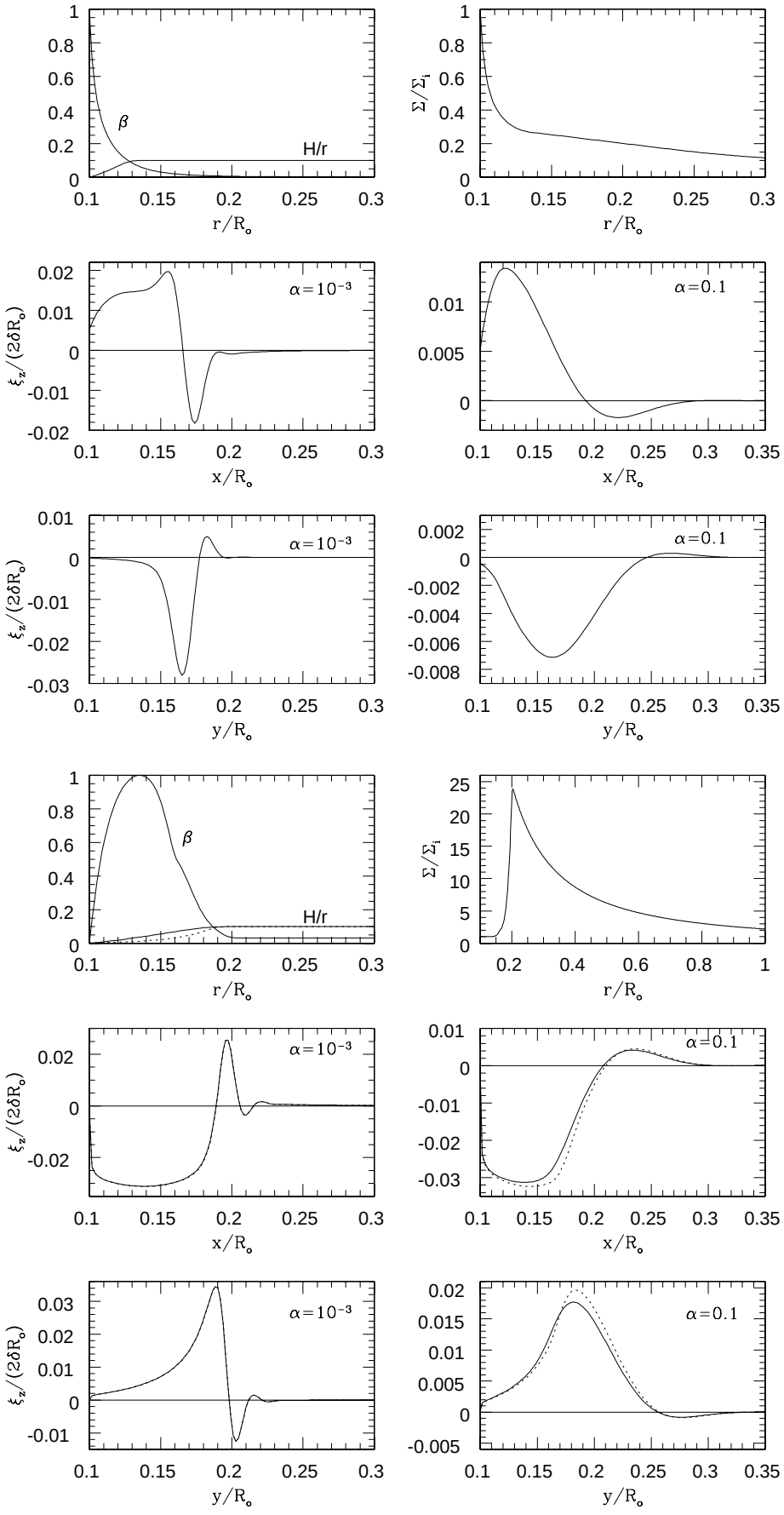

Fig. 2. Same as Fig. 1, but for a different magnetic support β and surface density Σ. Only one profile of H/r is considered here. Results are similar, although the maximum of $|\xi_z|$ is now closer to the disc inner edge.

Fig. 3. Same as Fig. 1, but for Low's magnetic field with $\varpi_B = 0.09999999$ and different magnetic support β and surface density Σ. The vertical displacement is almost constant and maximum very close to the disc inner edge, where it actually vanishes.

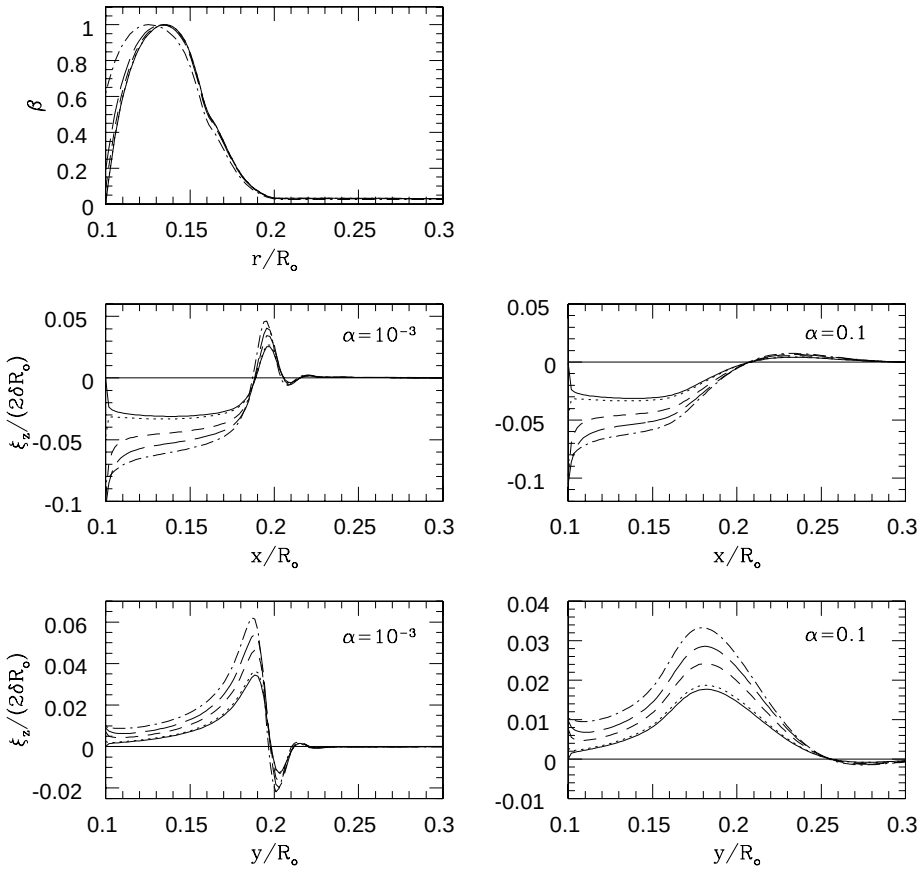

Fig. 4. Same as Fig. 3, but for different values of ϖ_B. The different curves correspond to $\varpi_B = 0.09999999$ (*solid lines*), 0.0999 (*dotted lines*), 0.099 (*short-dashed lines*), 0.0975 (*long-dashed lines*) and 0.09 (*dotted-dahed lines*). When ϖ_B is moved a little bit further away from the disc inner edge, the vertical displacement takes a finite value there.

Fig. 3 corresponds to Low's solution and $\varpi_B = 0.09999999$. Here again, the results hardly depend on the details of the profile of H/r in the disc inner parts. From Eq. (27), we see that ξ_z vanishes at $\varpi = \varpi_B$ if Σ is non zero there. When ϖ_B is very close to ϖ_i, we indeed check that ξ_z is almost zero at the disc inner edge. However, since B_r^+ varies very rapidly near ϖ_B, ξ_z takes some finite value at the inner edge as ϖ_B is moved a little bit away from ϖ_i. This is illustrated in Fig. 4, where we plot β and ξ_z for different values of ϖ_B, ranging from 0.09 to 0.09999999 (all the curves have the same parameters except for ϖ_B).

The calculations for the low viscosity $\alpha = 10^{-3}$ illustrate the excitation of bending waves. Several oscillations corresponding to bending waves excited at the OLR are visible. These are damped by viscosity before they propagate very far. This damping is enhanced by the increasing wavenumber produced by the decreasing magnetic field.

For larger and probably more realistic viscosity $\alpha = 0.1$, these waves are so heavily damped they are barely visible. The dominant displacement is near the disc inner edge in this case.

We note that, when viscous damping is present, the response of the disc is not in phase with the perturbation, and the warp lags behind the dipole. That is, the disc is also twisted, and the twist is trailing. Mathematically, this is illustrated by the fact that the imaginary part of ξ_z is non zero, as seen in the different figures. It may seem surprising that, even when α is as low as 10^{-3}, the imaginary part of ξ_z is comparable in magnitude to its real part. This is because ξ_z varies rapidly with radius when α is small, and the imaginary part of ξ_z becomes important when $|\partial^2 \xi_z / \partial r^2|$ is large (see Eq. [27]). We checked however that the imaginary part of ξ_z becomes very small compared to its real part when α is reduced further. Practically, the existence of a twist means that the point of maximum elevation in the disc is not in the plane which contains the dipole axis and the rotation axis of the star, i.e. the $(\varphi = 0)$, or equivalently (x, z), plane, but in a plane corresponding to a smaller (negative) φ. Or, in other words, the elevation does not vanish in the $(\varphi = \pi/2)$, or equivalently (y, z), plane, but in a plane corresponding to a smaller value of φ. To illustrate this, we show in Fig. 5 the line of nodes (which joins the points of zero elevation) in the inner parts of the (x, y) plane for both Aly's and Low's models and $\alpha = 0.1$. We clearly see that the line of nodes is trailing. If there were no twist, it would indeed coincide with the y–axis. The curves corresponding to different values of ϖ_B or different models are very similar to those displayed in Fig. 5. For $\alpha = 10^{-3}$, the line of nodes is more tightly wrapped, because ξ_z oscillates more rapidly.

In Fig. 6 we present a surface plot of the warped disc corresponding to the Low's model displayed in Fig. 3. This clearly shows the presence of an obscuring wall like feature near the disc inner boundary and the trailing twist.

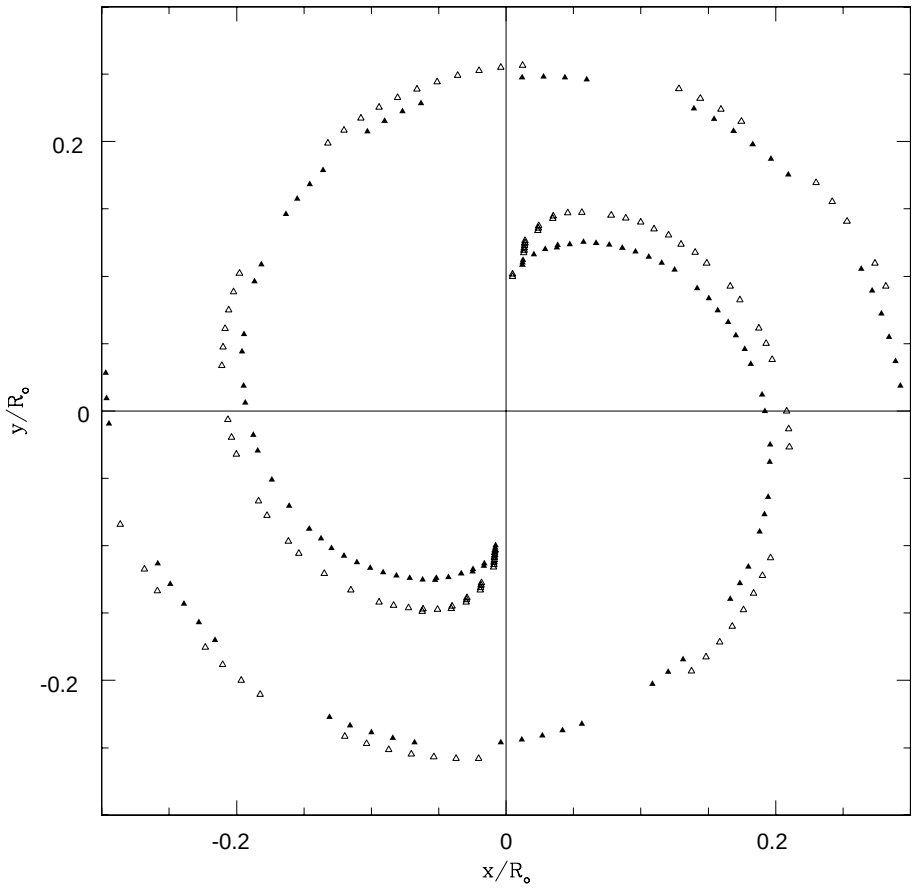

Fig. 5. Line of nodes in the inner parts of the (x, y) plane for the same models as Fig. 2 (Aly's magnetic field, *filled triangles*) and Fig. 3 (Low's magnetic field, *open triangles*). Here the profile of H/r is almost linear and $\alpha = 0.1$. We see that the line of nodes is trailing. If there were no twist, it would coincide with the y–axis. For $\alpha = 10^{-3}$, it is more tightly wrapped.

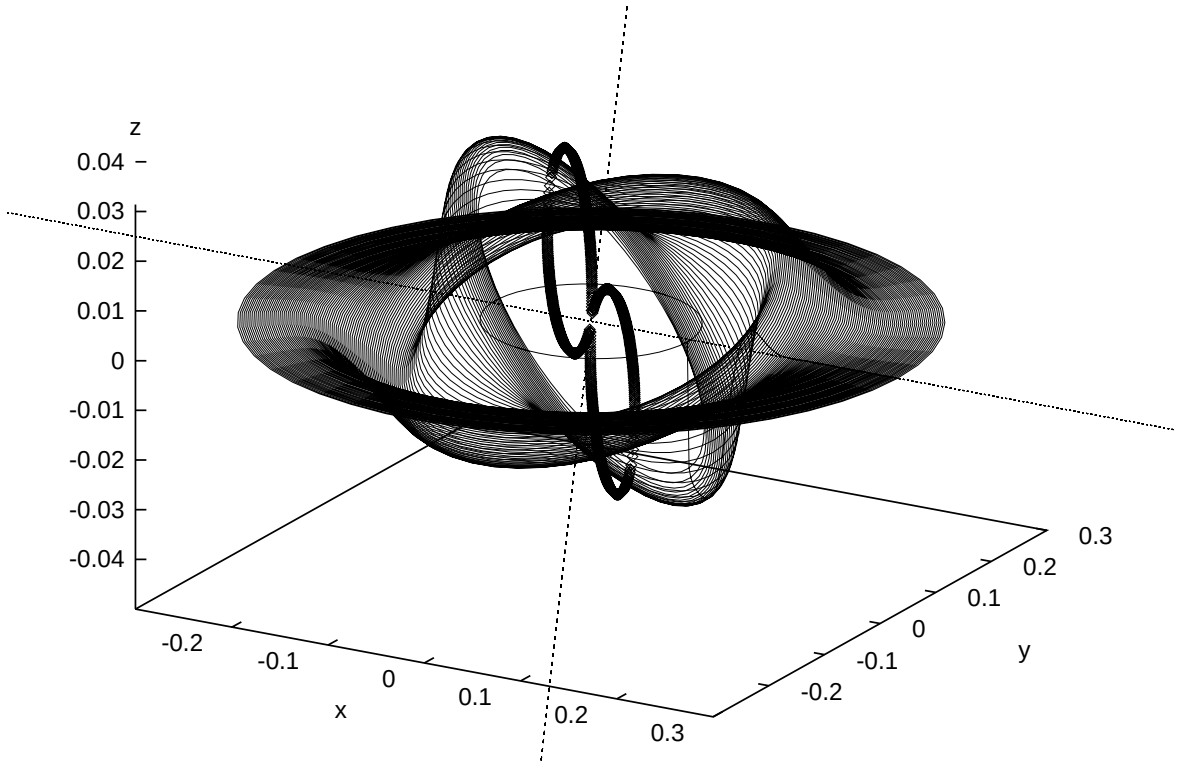

Fig. 6. 3D view of the disc corresponding to the model represented in Fig. 3 (Low's magnetic field). The dipole, its axis and the x–axis are also represented. The vertical scale has been amplified for clarity.

5. Discussion and application to AA Tau

The light curve of the classical T Tauri star AA Tau displays photometric, spectroscopic and polarimetric variations on timescales from a few hours to several weeks (Bouvier et al. 1999). The most striking feature of this light curve is a photometric variability with a period of 8 to 9 days, comparable to the expected rotation period of the star. This has been interpreted by Bouvier et al. (1999) as being due to the occultation of the star by a warp of the inner disc (the system is observed almost edge–on). They proposed that this warp be produced by the interaction of the disc with a stellar magnetic dipole tilted with respect to the disc rotation axis. Following Mahdavi & Kenyon (1998), they assumed that material at the disc inner edge, neglecting warping, would be more likely to accrete along the shorter field line than along the longer one connecting star and disc. In their model, based on this accretion geometry, the disc is elevated above the original equatorial plane at the location where the dipole axis is bent toward the disc. This geometry enables at least part of the stellar hot spots, located at the field line footpoints, to still be on the line of sight when occultation of the star is maximum, in agreement with the observations. In this model, the warp is not calculated self-consistently, and is not actually a real dynamical bending of the disc.

The assumption by Mahdavi & Kenyon (1998) can become incorrect, precisely because it neglects the warping of the disc. If the inner disc is no longer in the original equatorial plane, then material at the inner edge no longer 'sees' the short and long field lines it would see if it were in the unperturbed disc plane.

At the disc inner edge, since $\Omega(R_i) = \Omega_{\rm K}(R_i) = \omega$, we see from Eq. (27) that the sign of ξ_z is the same as that of P'_m (i.e., from Eq. [18], the same as that of $-B_r^+ B_r'^+$) for $\varphi = 0$, and that determines the direction in which the disc bends. From Fig. 3, we see that for Low's solution the disc inner edge on the x–axis is pushed below the equatorial plane, which is the opposite of what was anticipated by Mahdavi & Kenyon (1998). For Aly's solution, the disc is bent above the equatorial plane (see Fig. 1 and 2). It is not surprising that the two cases give different results since B_r^+ changes sign from one case to another.

To get the elevation of the disc above the equatorial plane, the real and imaginary parts of ξ_z have to be combined through Eq. (33). In Fig. 7, we show the maximum elevation $\xi_{z,max}$ (where the φ dependence has been taken into account in ξ_z), normalized to unity, above the equatorial plane along the $-\varphi$ direction, versus $-\varphi$. This represents the maximum elevation of the disc material located in between the star and an observer looking at the disc almost edge–on and from above along the $-\varphi$ direction. The curves correspond to Aly's and Low's models displayed in Fig. 1 and 3, respectively, and $\alpha = 0.1$. Let us suppose that, to begin with, we look at the system along the $\varphi = 0$ direction. Then, as the star rotates, our line of sight moves to smaller, negative values of φ (to the right along the x–axis of Fig. 7). In the case of Aly's model, this corresponds to the star being occulted at first and until it has rotated by about 90 degrees. Then, as the star rotates further, it becomes less and less obscured, and it can be seen by the observer until it has completed a full rotation. In the case of Low's model, the star is not obscured at first. Occultation begins only after the star has rotated by about 180 degrees and lasts also for about a quarter of a period. We note that, depending on the direction of the line of sight, the radius at which the elevation is maximum varies (typically between 0.1 R_o and 0.2 R_o). It is unlikely that the observer would be able to know at which radius is the part of the disc responsible for the occultation, as the whole structure rotates with the same frequency (that of the star). Indeed, it is important to stress again that a structure located at some radius r does not rotate with the local angular frequency but with that of the star (in other words, the warp appears steady in a frame rotating with the star).

With Low's solution, the disc is pushed below the equatorial plane at the location where the dipole is bent toward the disc. Therefore the stellar hot spots, at the field line footpoints cannot be seen under condition of maximum occultation, unless they are relatively large. In Aly's case, at least part of the hot spots can still be observed at an occultation maximum because of the phase–lag between the disc response and the perturbation.

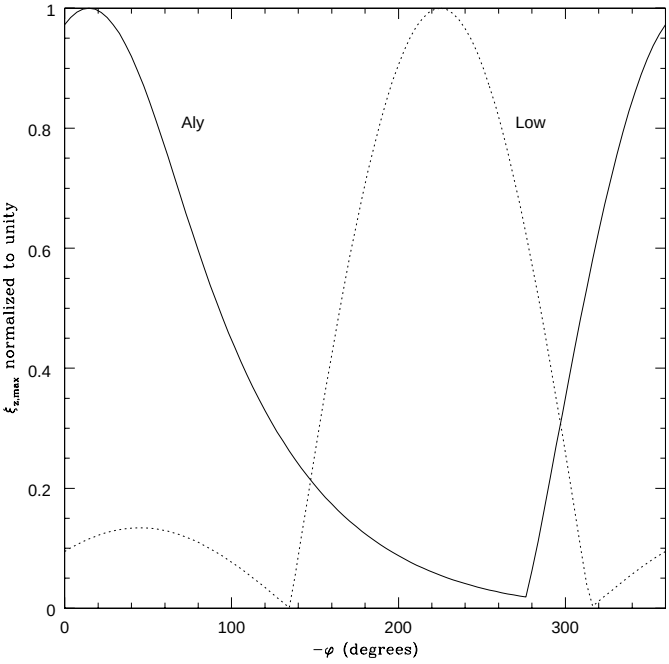

Fig. 7. Maximum elevation $\xi_{z,max}$ (where the φ dependence has been taken into account in ξ_z), normalized to unity, above the equatorial plane along the $-\varphi$ direction, versus $-\varphi$ in degrees. This represents the maximum elevation of the disc material located in between the star and an observer looking at the disc almost edge–on and from above along the $-\varphi$ direction. The curves correspond to the models shown in Fig. 2 (Aly's magnetic field, *solid line*) and Fig. 3 (Low's magnetic field, *dotted line*). Here the profile of H/r is almost linear and $\alpha = 0.1$. Depending on the direction of the line of sight, the radius at which the elevation is maximum varies (typically between 0.1 R_o and 0.2 R_o). For Aly's model, maximum occulation occurs for φ in the range $[-\pi/2, 0]$, whereas for Low's model it occurs for φ in the range $[-3\pi/2, -\pi]$ or, equivalently, $[\pi/2, \pi]$.

Indeed, we see in Fig. 7 that, for the particular Aly's model represented there, the occultation is maximum when $\varphi \sim -15°$, and not when $\varphi = 0$. Therefore, it seems the observations favour Aly's model.

To fit the observations, Bouvier et al. (1999) needed the amplitude of the warp to be about 0.3 times the disc inner radius. We see from Figs. 1–3 that this is easily attained here. There, noting that $R_i/R_o = 0.1$, $|\xi_z|/(2\delta R_i)$ ranges from about 0.1 to 1. For δ up to about $30°$ (for which $\sin\delta \simeq \delta$ in radians), this gives $|\xi_z|/R_i$ from 0.1 to 1. The lower value could even be made larger by considering a profile of H/r with an exponential rather than almost linear increase in Fig. 2. Therefore only a moderate misalignment angle is required to produce $|\xi_z|/R_i \sim 0.3$.

Figs. 1–3 show that when the viscosity in the disc is small ($\alpha = 10^{-3}$ for instance), the vertical displacement of the disc varies rapidly, on a scale smaller than the disc semi–thickness H. In that case, we expect the warp to become dispersive (Papaloizou & Lin 1995), and probably the disc to disrupt. It is likely that different situations arise when a disc interacts with a nonaligned dipole, depending on the detailed physics. In some cases we may get a moderate smoothly varying warp, as described above, in other cases it may be that the disc breaks up and reforms. This may also produce light curve variability.

We note that the bending waves which are excited by the tilted dipole transport angular momentum (Papaloizou & Terquem 1995; Terquem 1998), which is deposited in the disc if the waves are damped. Since the dipole rotates faster than the disc in which the waves propagate, the resulting torque opposes accretion onto the star. This effect may produce additional variability, and will be the subject of another paper.

Acknowledgements. It is a pleasure to thank Jérôme Bouvier for many interesting and stimulating discussions about AA Tau and for useful comments on an earlier draft of this paper, and Claude Bertout for further information about the variability of CCTS. We also thank an anonymous referee and A. P. Goodson whose suggestions helped to improve the quality of this paper. JCBP is grateful to the Laboratoire d'Astrophysique de l'Observatoire de Grenoble for hospitality and visitor support. CT is grateful to the Astronomy Unit at QMW for hospitality and visitor support through PPARC grant PPA/V/O/1997/00261.

References

Agapitou V., Papaloizou J.C.B., Terquem C., 1997, MNRAS 292, 631
Aly J.J., 1980, A&A 86, 192
Balbus S.A., Hawley J.F., 1998, Rev. Mod. Phys. 70, 1
Bertout C., Basri G., Bouvier J., 1988, ApJ 330, 350
Bouvier J., Cabrit S., Fernandez M., Martín E.L., Matthews J.M., 1993, A&A 272, 176
Bouvier J., Chelli A., Allain S., et al., 1999, A&A 349, 619
Brandenburg A., Tuominen I., Moss D., 1989, Geophys. Astrophys. Fluid Dyn. 49, 129
Brandenburg A., Nordlund A., Stein R., Torkelsson U., 1995, ApJ 446, 741
Edwards S., Strom S.E., Hartigan P., Strom K.M., Hillenbrand L.A., 1993, AJ 106, 372
Edwards S., Hartigan P., Ghandour L., Androulis C., 1994, AJ 108, 1056
Ghosh P., Lamb F.K., 1979, ApJ 232, 259
Ghosh P., Lamb F.K., 1991, In: Ventura J., Pines D. (eds.) Neutron stars: Theory and observation. Kluwer, Dordrecht, p. 363
Goldreich P., Tremaine S., 1978, Icarus 34, 240
Goodson A.P., Winglee R.M., Boehm K.-H., 1997, ApJ 489, 199
Guenther E.W., Lehmann H., Emerson J.P., Staude J., 1999, A&A 341, 768
Hartmann L., Hewett R., Calvet N., 1994, ApJ 426, 669
Hawley J.F., Gammie C.F., Balbus S.A., 1995, ApJ 440, 742
Hawley J.F., 2000, ApJ 528, 462
Hayashi M.R., Shibata K., Matsumoto R., 1996, ApJ 468, L37
Johns-Krull C., Valenti J.A., Hatzes A.P., Kanaan A., 1999, ApJ 501, L41
Königl A., 1991, ApJ 370, L39
Kudoh T., Matsumoto R., Shibata K., 1999, In: Nakamoto T. (ed.) Star Formation 1999. p. 286
Lai D., 1999, ApJ 524, 1030
Low B.C., 1986, ApJ 310, 953
Mahdavi A., Kenyon S.J., 1998, ApJ 497, 342
Mikic Z., Linker J.A., 1994, ApJ 430, 898
Miller K.A., Stone J.M., 1997, ApJ 489, 890
Montmerle T., Feigelson E.D., Bouvier J., Andr'e P., 1994, In: Levy E.H., Lunine J.I. (eds.) Protostars and Planets III, Univ. Arizona Press, Tuscon, p. 689
Najita J., Edwards S., Basri G., Carr J., 2000, In: Mannings V., Boss A.P., Russell S.S. (eds.) Protostars and Planets IV, University of Arizona Press, Tucson, in press
Papaloizou J.C.B., Lin D.N.C., 1995, ARA&A 33, 505
Papaloizou J.C.B., Pringle J.E., 1983, MNRAS 202, 1181
Papaloizou J.C.B., Terquem C., 1995, MNRAS 227, 553
Shakura N.I., Sunyaev R.A., 1973, A&A 24, 337
Shu F.H., 1984, In: Greenberg R., Brahic A. (eds.) Planetary Rings. Univ. Arizona Press, Tuscon, p. 513
Spruit H.C., Stehle R., Papaloizou J.C.B., 1995, MNRAS 275, 1223
Tagger M., Henriksen R.N., Sygnet J.F., Pellat R., 1990, ApJ 353, 654
Tayler R.J., 1987, MNRAS 227, 553
Terquem C.E.J.M.L.J., 1998, ApJ 509, 819
Wang Y.-M., 1995, ApJ 449, L153